

Electromechanical transient modeling of energy storage based on virtual synchronous machine technology

JUNTAO CUI¹, ZHAO LI², PING HE² ✉, ZHIJIE GONG², JIE DONG²

¹Lanzhou Resources and Environment Voc-Tech University
China

²Zhengzhou University of Light Industry
China

e-mail: hplkz@126.com

(Received: 19.07.2021, revised: 03.03.2022)

Abstract: This paper proposes an electromechanical transient method to build a battery energy storage system-based virtual synchronous generator model, suitable for a large-scale grid. This model consists of virtual synchronous generator control, system limitation and the model interface. The equations of a second-order synchronous machine, the characteristics of charging/discharging power, state of charge, operating efficiency, dead band and inverter limits are also considered. By equipping the energy storage converter into an approximate synchronous voltage source with an excitation system and speed regulation system, the necessary inertia and damping characteristics are provided for the renewable energy power system with low inertia and weak damping. Based on the node current injection method by the power system analysis software package (PSASP), the control model is built to study the influence of different energy storage systems. A study on the impact of renewable energy unit fluctuation on frequency and the active power of the IEEE 4-machine 2-area system is selected for simulation verification. Through reasonable control and flexible allocation of energy storage plants, a stable and friendly frequency environment can be created for power systems with high-penetration renewable energy.

Key words: battery energy storage system, electromechanical transient model, virtual synchronous machine

1. Introduction

With the increasing penetration of inverter-based devices in the modern generation grid, a large number of generators are replaced by environment-friendly renewable energy systems (RESs), and grids are changing from traditional to clean, efficient and intelligent. However, the negative



© 2022. The Author(s). This is an open-access article distributed under the terms of the Creative Commons Attribution-NonCommercial-NoDerivatives License (CC BY-NC-ND 4.0, <https://creativecommons.org/licenses/by-nc-nd/4.0/>), which permits use, distribution, and reproduction in any medium, provided that the Article is properly cited, the use is non-commercial, and no modifications or adaptations are made.

effect of inverter-based renewable energy sources on the power system stability is considerable since they don't contribute to inertia and damping as traditional synchronous generators [1]. Many of these insufficiencies are caused by the lack of synchronization stability within inverter-based devices. Renewable energy sources must sacrifice output power to get in return stability. To run closer to full capacity during operation, additional energy storage within grids is a key element in adding more renewable energy sources [2]. Energy storage technology, with its flexible layout as well as intelligent charging and discharging energy supply, will penetrate into all aspects of the system such as power generation, transmission, distribution, consumption, thus changing the traditional mode of instantaneous supply and demand balance of the existing playing system [3].

Due to the fact that the battery energy storage system (BESS) generally plays an important role in balancing energy fluctuations in the system frequency regulation, numerous studies have been developed on the BESS [4]. The role of the BESS is even more important for enhancing the stability of the future grid characterized by low system inertia [5]. In order to improve the response rate and power supply capacity, energy storage is required to provide valuable benefits such as improved stability and power quality [6]. Droop control is a conventional method for grid-scale BESSs to mitigate the negative impacts of renewable resources by regulating both voltage and frequency simultaneously [7]. Based on this, the models used in the BESS are often developed to meet the specific control objectives. Fast-responding storage devices can mimic inertial responses through some specified control algorithm [8]. Virtual inertia is a control algorithm that combines the RES, BESS, and power electronics to emulate the inertia of the traditional power system [9]. It can be used to enhance the inertia of the system, which is one of the effective methods to maintain frequency stability, but the ability to provide virtual damping might be insufficient in the low damping system [10]. To address this issue, virtual synchronous generator (VSG) control imitates the dynamic performance of synchronous generators to improve system characteristics. By using short-term energy storage together with a power inverter and proper control mechanism, the VSG can be established to support grid control [11]. The VSG technology introduces the basic theory and operation experience of SGs into the design of a grid connection algorithm to resolve the problems caused by low damping and inertia [12]. However, the VSG control is mainly applied to microgrids with an electromagnetic transient model, and there are still few studies on establishing energy storage-based VSG control in large-scale grids [13–15].

In this paper, the structure of the BESS and the VSG control is analyzed, then proposes an electromechanical transient model of the BESS with the VSG control that is suitable for large-scale power grids. The model of the BESS contains a power control module, ontological model and grid interface. Then the effectiveness of the model is verified by a user-defined model in the power system analysis software package (PSASP) and its performance is compared with droop control under the system's fluctuation. Finally, the model is operated in provincial power grids and general configuration suggestions are given.

2. Principle of VSG

The structure based on the VSG is shown in Fig. 1. The energy storage unit is connected to the grid through the grid-connected inverter with the VSG control strategy and then flows into the grid through the LCL-filter and transmission line. i_{abc} is the grid-connected current, u_{abc} , e_{abc}

and u_{mabc} are the induced electromotive force, output voltage and voltage modulation signals, respectively. T_m is the mechanical torque, P and Q are the actual output active power and reactive power of the VSG, respectively.

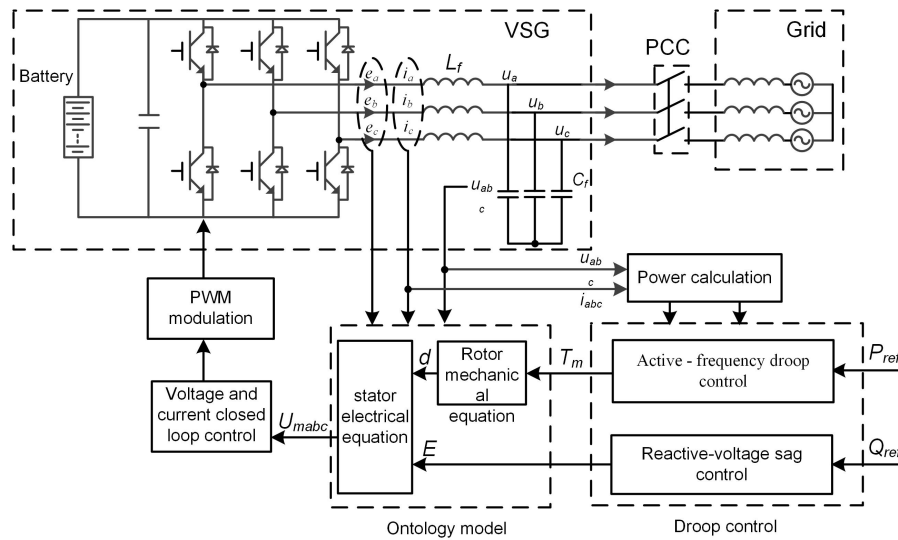


Fig. 1. VSG control structure diagram

It can be seen from Fig. 1 that the inverter control strategy consists of droop control, the ontology model and closed-loop control. The inner-loop instruction voltage u_{mabc} is calculated by the droop control and VSG ontology model, and then the output is made to track the command voltage without difference by the internal loop control.

The active power control of the VSG is composed of $P-\omega$ droop control and rotor mechanical equations. The $P-\omega$ droop control simulates the governor from the external characteristics, which makes active power and system frequency have droop characteristics. However, droop control is a differential power control method, in which it is difficult to meet the control objectives when the VSG controls micro-source grid connection. Therefore, in this paper, the fixed active-frequency and reactive-voltage droop coefficients are replaced by the proportional-integral link to realize VSG control without static error. The expression is as follows:

$$\begin{cases} P_m = P_{ref} + \left(k_f + \frac{k_{fi}}{s}\right) \cdot \Delta\omega, \\ \Delta\omega = \omega_n - \omega \end{cases}, \quad (1)$$

where: $\Delta\omega$ represents the frequency deviation between the reference frequency ω_n and the angular frequency ω , k_f is the proportion coefficient of active droop, k_{fi} is the integral coefficient of active droop control, P_m and P_{ref} are the reference values of mechanical power and active power, respectively.

The rotor equation regulates the frequency by the power difference $P_m - P_e$, and the damping power is used to suppress power oscillation. The formula is as follows:

$$\begin{cases} J \frac{d(\omega - \omega_0)}{dt} = \frac{P_m}{\omega_n} - \frac{P_e}{\omega_n} - D(\omega - \omega_n) \\ \frac{d\delta}{dt} = \omega - \omega_n \end{cases}, \quad (2)$$

where: D is the damping factor, $D(\omega - \omega_n)$ is the damping power, P_m is the mechanical power of the swing equation, P_e is the electrical power generation and J is the virtual inertia. It can be seen from the above formula that J makes the dynamic characteristics of power and frequency inertial, while D improves the system damping and generates damping power to suppress oscillations during fluctuations.

The reactive power control of the VSG is shown in (3). The voltage amplitude is adjusted by the bus voltage difference as well as reactive power deviation as feedback, and then the electric potential of the VSG is obtained by simulating the excitation system through a proportional integration link [16].

$$\begin{cases} E = E_0 + \left(k_q + \frac{k_{qi}}{s}\right) \times \Delta Q + \left(k_v + \frac{k_{vi}}{s}\right) \times \Delta U \\ \Delta Q = Q_{\text{ref}} - Q_e \\ \Delta U = U_{\text{ref}} - U \end{cases}, \quad (3)$$

where k_v and k_{vi} are the reactive voltage proportionality factor and reactive voltage integration factor, respectively. k_q is the reactive power proportionality factor; k_{qi} is the reactive power integration factor; E is the internal potential of the VSG; ΔQ is the difference between the reference reactive power Q_{ref} and reactive power Q_e ; ΔU is the difference between the reference grid voltage U_{ref} and the grid voltage U ; E_0 is the amplitude of the no-load electric potential output from the VSG.

To achieve $P-Q$ decoupling control, the requirement for VSG operation is that the transmission line impedance $R + jX$ is close to pure inductance. Therefore, the virtual resistance R is made zero, so that the equivalent impedance between the inverter output voltage and the grid voltage behaves as pure inductance. The grid-connected current and output apparent power is shown in (4)

$$\begin{cases} i = \frac{E \angle \delta - U \angle 0}{R + jX} \\ S = UI^* = U \frac{E \angle (-\delta) - U}{-jX} = P + jQ \end{cases}. \quad (4)$$

By expanding the above equation, the grid-connected injected active power and reactive power of the converter can be written as:

$$P = \frac{EU \sin \delta}{X}, \quad (5)$$

$$Q = \frac{EU \cos \delta - U^2}{X}. \quad (6)$$

3. Construction of energy storage model controlled by VSG

3.1. Energy storage system model structure

Compared with the precise electromagnetic transient model, the electromechanical transient model of energy storage is more suitable for the transient processes analysis and control of large-scale grid-connected systems. The control model of the BESS consists of the grid-connected converter, energy storage ontology model and interface, as shown in Fig. 2. The control structure of the grid-connected converter is generally divided into inner and outer loop control. The outer loop control is the main controller of the system. After reading the frequency ω and voltage amplitude V from the grid, the active power command P_{set} and reactive power instruction Q_{set} are calculated according to the control strategy. The active power P and reactive power Q of the converter obtained through the inner loop control link are injected into the grid as the d -axis component i_d and the q -axis component i_q of the energy storage AC side current through the model interface.

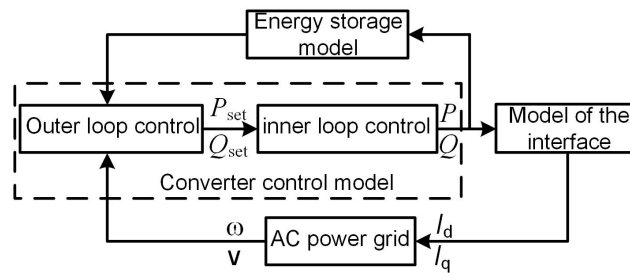


Fig. 2. Control model of energy storage system

3.2. Model of energy storage grid-connected converter

The power converter system (PCS) of energy storage is the core of the energy storage system, whose purpose is to control the inverter circuit and to adjust the frequency, amplitude and phase, to realize the conversion between the direct current of the energy storage and the alternating current suitable for grid-connection. The external characteristics of energy storage are closely related to the control strategy of the converter. According to the system requirements, the outer loop control can be set to droop control, constant reactive power control, constant voltage control, constant power factor control, VSG control, etc. According to the active power and reactive power instructions issued by the outer loop, the inner loop control can achieve four-quadrant power regulation through pulse width modulation (PWM). Figure 3 shows the control model of the energy storage converter under a VSG algorithm. After reading bus frequency, power and voltage from the grid, the power outputs P_{set} and Q_{set} of the outer loop can be obtained as command power. Then the actual output active power P and reactive power Q of the energy storage system are obtained by inner loop control of the converter.

The structure of the inner loop is mainly composed of the inner loop model of the feedforward decoupling method based on the PI link and the voltage source converter (VSC). By adjusting the

voltage reference value of the inner loop output, the AC side current can track the output current instruction of the outer loop control. Active and reactive power decoupling control is used to eliminate coupling.

After combining the equivalent transformations of the converter and inner loop control models, independent control loops with d and q axes can be obtained. Based on this, according to the zero-pole cancellation principle, the transfer function can be approximately considered a first-order inertial link. The power characteristics are as follows:

$$\begin{cases} \frac{dP}{dt} = -\frac{P}{T} + \frac{P_{set}}{T} \\ \frac{dQ}{dt} = -\frac{Q}{T} + \frac{Q_{set}}{T} \end{cases}, \quad (7)$$

where T is the response time of tracking P and Q by P_{set} and Q_{set} .

The overall structure of the outer loop control strategy of the energy storage controller is shown in Fig. 3, and each energy storage module is built based on the user-defined model in the PSASP.

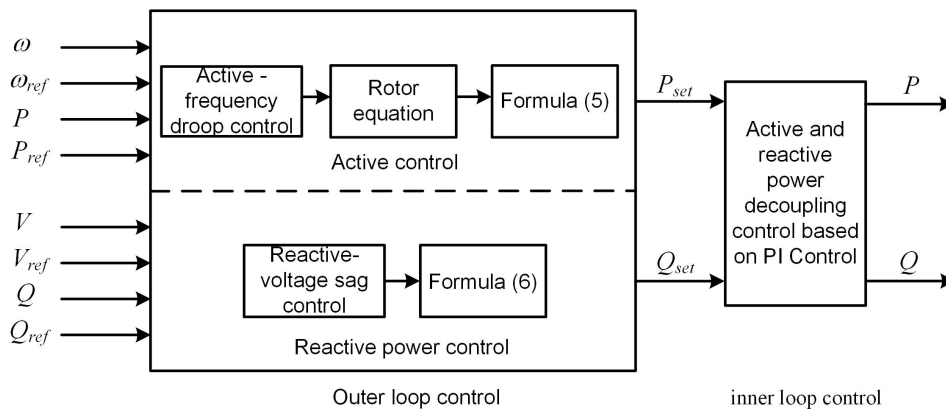


Fig. 3. PCS model controlled by VSG

To realize the effect of the BESS providing inertia and damping for the grid, the power control is established as shown in Fig. 4 and the active power control part is shown in Fig. 4(a). The block diagram shows the active frequency control, rotor equation and active power output corresponding to Eqs. (1), (2) and (5) from top to bottom, where the on-chip memory bus (OMB) is the bus frequency and PG_0 is the initial value of active power. The meanings of each function box and signals in Fig. 4–6 can be seen in the literature [17]. Table 1 shows the meaning of temporary convention variables TM1-TM10. The reactive power control is shown in Fig. 4(b), and the two-block diagrams correspond to (3) and (6), respectively. QG_0 is the initial value of reactive power; VT is the bus voltage; VT_0 is the initial value of bus voltage.

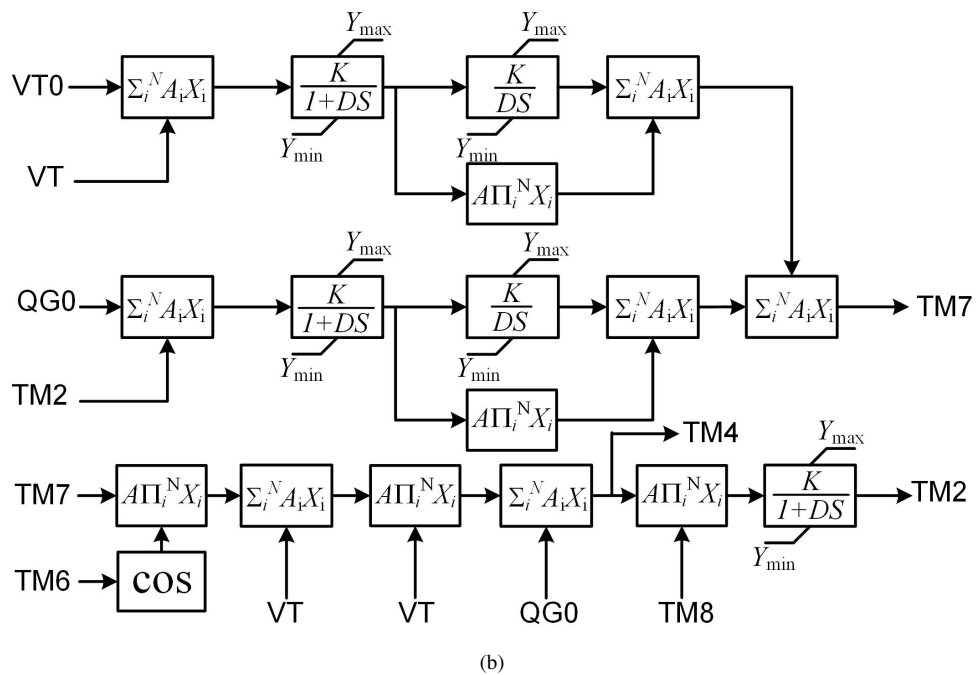
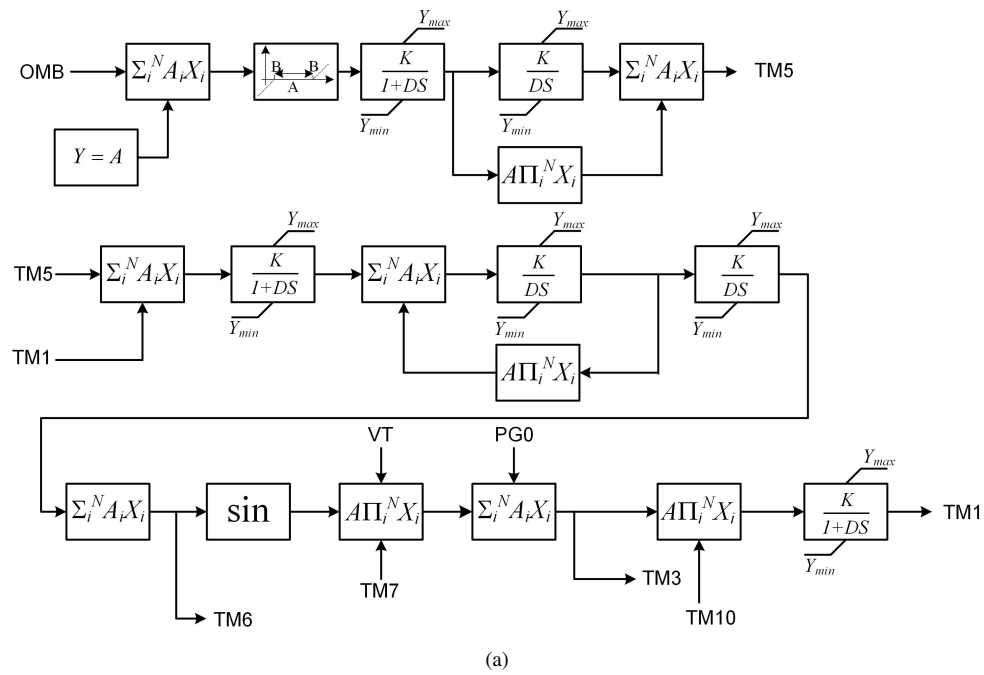


Fig. 4. Outer loop power control module: active power control regulation (a); reactive power control regulation (b)

Table 1. Temporary convention variable setting description

Temporary contract variable	Functional specifications
TM1	actual output active power P
TM2	actual output reactive power Q
TM3	active power instruction P_{set}
TM4	reactive power instruction Q_{set}
TM5	mechanical power P_m
TM6	power angle δ
TM7	inner electric potential E
TM8	reactive power control signal
TM9	state of charge
TM10	active power control signal

3.3. Energy storage model construction based on VSG

The energy storage model includes state of charge (SOC) calculation, capacity limitation, the dead-band link, operating efficiency, charging/discharging power limit and converter capacity limit. Since this paper focuses on the comparison between VSG control and the existing general model for improving grid fluctuation, a simplified internal energy storage model is established.

1. SOC refers to the percentage of existing power and the maximum amount of the battery capacity, which reflects the amount of remaining battery capacity. It plays an important role in the utilization efficiency and the service life of the battery. Commonly used methods for estimating SOC include the ampere-hour integration method, open-circuit voltage method and neural network method, Kalman filtering algorithm, etc. [18]. This paper uses the widely used and simple ampere-hour measurement method to estimate SOC.
2. Energy storage capacity limitation also means maintaining the SOC of the BESS within a reasonable range to prevent battery damage from overcharging.
3. Charge and discharge power limits are due to the constraints of energy storage components, resulting in the existence of charge and discharge power upper and lower limits of the energy storage system.
4. The operating efficiency of the BESS includes the single operating efficiency and power electronics device efficiency. In this paper, the effect of the change of the battery charge state on the energy storage operation efficiency is simplified, and the overall operational efficiency is simplified to a constant.
5. Converter capacity limitation refers to the fact that most of the stored active power cannot be filled with power capacity, so the converter has a certain reactive power regulation ability, which is often dominated by active power and supplemented by reactive power [19].
6. The dead band is an artificial boundary, which can avoid frequent charging and discharging of the BESS when the system is subjected to small disturbance and reduce the energy storage life [20].

According to the above principles, the constraints can be listed as follows:

$$\left\{ \begin{array}{l} \text{SOC} = \text{SOC}_0 + \frac{\int_0^t P_{\text{set}} dt}{\text{SOC}_{\text{tot}}} \\ \text{If } \text{SOC} \notin [\text{SOC}_{\text{min}}, \text{SOC}_{\text{max}}], P = 0 \\ P_{\text{max}} \leq P \leq P_{\text{max}} \\ Q_{\text{max}} \leq Q \leq Q_{\text{max}} \\ Q_{\text{max}} = \sqrt{S^2 - P^2} \\ P = \eta P_{\text{set}} \\ \text{If } f \in [f_{\text{min}}, f_{\text{max}}], P = 0 \end{array} \right. , \quad (8)$$

where: SOC is the total capacity of the battery; SOC_0 is the initial SOC; the active power reference P_{set} is the active power issued by energy storage components, including the active power P and power loss output to the grid. The active power P is positive in charging and negative in discharging, which is limited by the maximum charging and discharging power of energy storage, while the reactive power Q is limited by the capacity of the inverter. The main parameters of energy storage are shown in Table 2. By setting the active power control model parameters in Fig. 4(a), the charging/discharging power limitation, energy storage operation efficiency and dead band are realized. The SOC calculation, capacity limit and converter limiting modules are shown in Fig. 5.

Table 2. Energy storage parameter setting

Parameter	Numerical value
overall operating efficiency of energy storage system η	0.85
initial state of charge SOC_0	0.6
minimum state of charge SOC_{min}	0.2
maximum state of charge SOC_{max}	0.8
total capacity SOC_{tot} (discharge time under rated power)	200
maximum active output of energy storage P_{max}	0.1
minimum frequency dead band f_{min}	49.96
maximum frequency dead band f_{max}	50.033

3.4. Model of the interface

Since the PSASP is based on the nodal current injection method to inject the model output power into the system, the active power P as well as reactive power Q generated from the inner

loop need to be transformed into the form of the current real component I_r and current imaginary component I_i .

The energy storage model injects power into the system, which can be read from the nodal bus voltages. The real part of the current is U_r and the imaginary part is U_i . Then, by using the inverse solutions of P and Q , the apparent power I_r and I_i can be calculated.

$$\begin{cases} S = UI^* = (U_R + jU_I)(I_R - jI_I) = P + jQ \\ I_R = \frac{U_R P + U_I Q}{U_R^2 + U_I^2} \\ I_I = \frac{U_I P - U_R Q}{U_R^2 + U_I^2} \end{cases} \quad (9)$$

According to this formula, the grid-connected interface model of the PSASP can be drawn as shown in Fig. 5. VT1R and VT1I correspond to the real part U_R and imaginary part U_I of the bus voltage, respectively; ITR and ITI correspond to I_r and I_i , respectively.

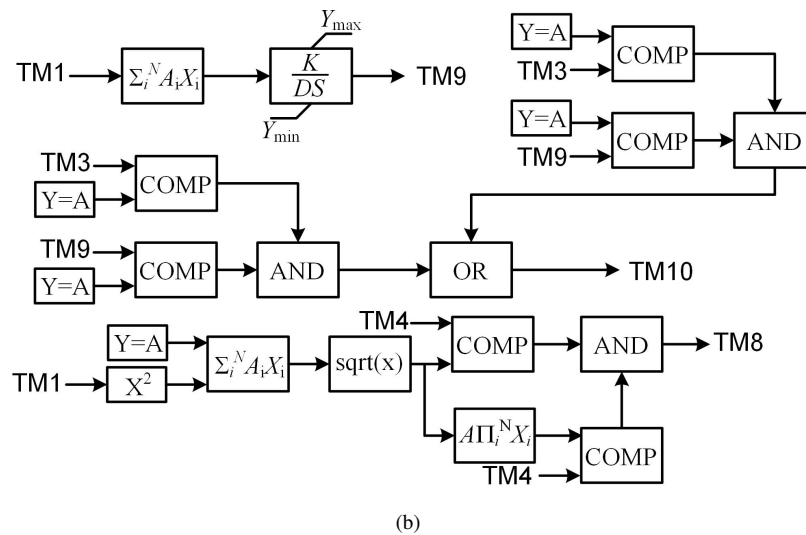
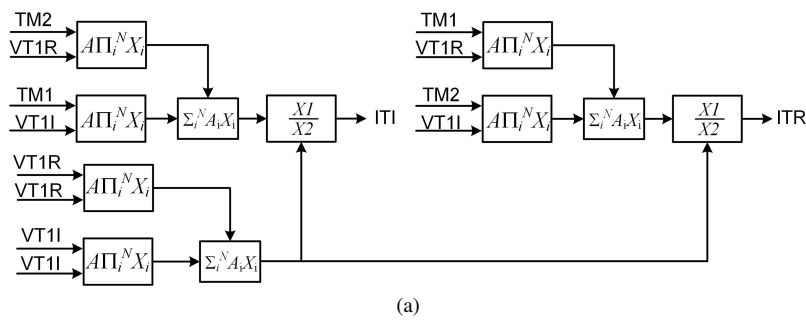


Fig. 5. BESS model: grid interface model (a); energy storage restriction link (b)

4. Case study

In order to verify the effectiveness of the model constructed in this paper, the wind farm power plants, photovoltaic power stations and energy storage are added to the IEEE 4-machine-2-area system for analysis. The structure of the grid is shown in Fig. 6 and the detailed generator parameters are shown in Table 3.

Table 3. Generator parameter setting

	x_d	x'_d	x''_d	x_q	x'_q	x''_q	T'_{d0} (s)	T''_{d0} (s)	T'_{q0} (s)	T''_{q0} (s)	H_g (s)
G ₁ , G ₂	1.8	0.3	0.25	1.7	0.55	0.25	8	0.03	0.4	0.05	12.35
G ₃ , G ₄	1.8	0.3	0.25	1.7	0.55	0.25	8	0.03	0.4	0.05	13

The generators G₁ and G₂ in area 1 and generators G₃ and G₄ in area 2 are connected by double loop tie lines. The rated capacity of four generators is 900 MVA, of which each generator outputs 700 MW and the grid-connected voltage is 20 kV. The transmission power of the tie line is 400 MW and the generator G₃ is the balance node. The energy storage plant is connected to bus 6, and the steady-state output power is 0. The photovoltaic plant and wind farm are connected to bus 10, and their steady-state output power is 48 MW and 30 MW, respectively.

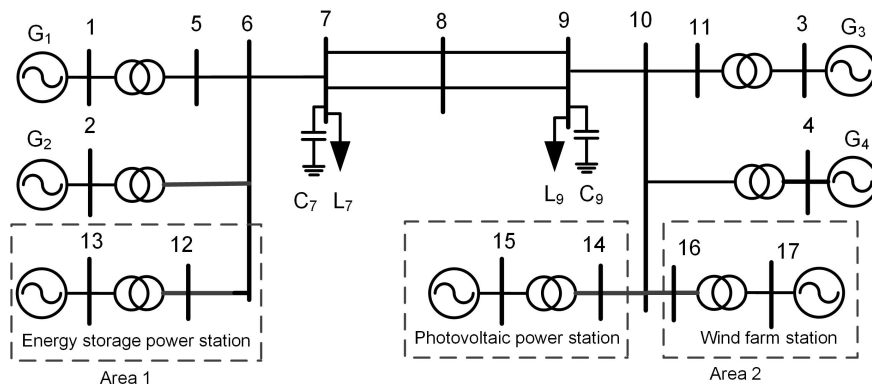


Fig. 6. IEEE Four-machine two-zone system

In order to verify the effectiveness of VSG control and droop control with an energy storage model suppressing the fluctuations of new energy, this paper sets the VSG energy storage model as model 1, the droop control based on an energy storage electromechanical transient model as model 2, and the energy storage model in PSASP software as model 3. By observing the generator power angle, bus voltage, transmission power, output power of the BESS and the oscillation characteristics of the system under various operating conditions, the conclusion is drawn.

4.1. Influence of different energy storage on the system of new energy units during wind-solar fluctuation

In the simulation, the wind farm is disturbed by gusts at $t = 2$ s and the wind speed starts to increase. The wind speed increases by 8 m/s and reaches the maximum value at $t = 3$ s. After that, the gust gradually weakens, and the wind speed returns to the initial level at $t = 4$ s. For the photovoltaic power station, it began to be disturbed by the gradual light at $t = 1$ s, and the light intensity increased at a rate of 5 w/m^2 . After reaching the maximum value at $t = 3$ s, it remains unchanged until it starts to decrease at the same rate at $t = 4$ s, and the light intensity returns to its initial value at $t = 6$ s.

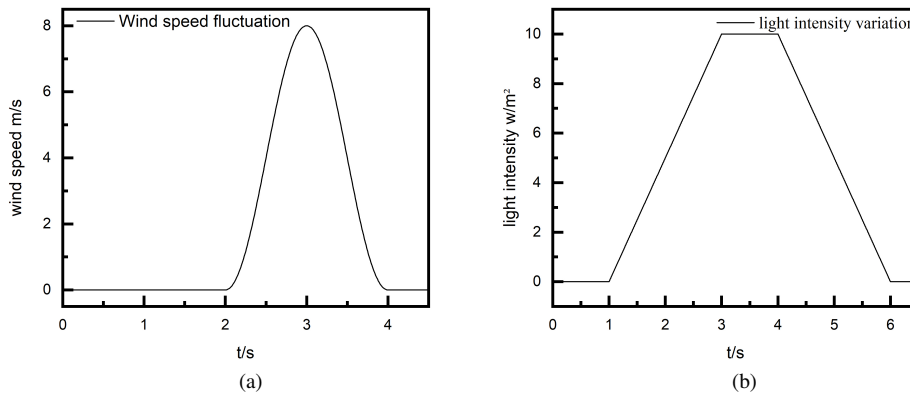


Fig. 7. Disturbance of wind farms and photovoltaic power plants: wind speed fluctuations in wind farms (a); changes in light intensity (b)

From the simulation results of Fig. 8, it can be seen that model 1 and model 2 have a significant effect on suppressing oscillation fluctuations under the disturbance of wind speed and light intensity, while model 3 has a weaker effect on improving output fluctuations of renewable energy power stations. Both model 1 and model 2 have good effects on the response curves of generator phase angle, bus voltage and tie-line transmission power, and the stability of the system is significantly improved. Moreover, model 1 can recover the oscillation faster and the fluctuation range of the curve is smaller, so the effect of suppressing the fluctuation is the best.

Furthermore, in order to reflect the improvement of the VSG control strategy on the system stability, Prony analysis is performed for the energy storage-based VSG control system and the energy storage-based droop control respectively. The oscillation frequency, damping, amplitude and characteristic root of the system are estimated by analyzing the modalities of the response curve. The perturbation is set as the load 1 active power step response to reduce the effect of noise on the fitting results. The results are shown in Table 3, where model 1 is the inter-regional oscillation, model 2 is the local oscillation of area 1, and model 3 is the local oscillation of area 2.

The partial results of eigenvalues oscillation modes and dominant eigenvalues (λ), damping (ζ), frequency as well as attenuation coefficients are shown in Table 4. It is known that compared to model 3, model 1 and model 2 have significant improvement effects on the system oscillation. For example, the damping ratio as well as the frequency of the inter-regional oscillation increase significantly, and model 2 has the best effect on suppressing oscillations. For the

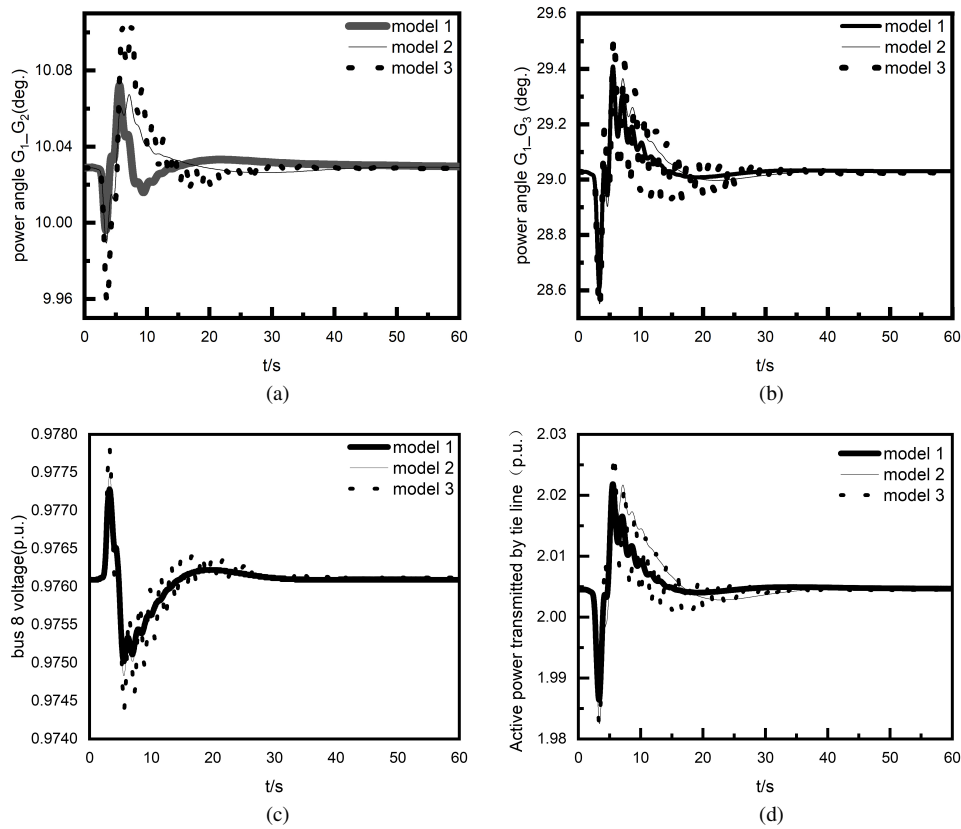


Fig. 8. Oscillation curve of the system with different energy storage added: power angle of generator $G_1_G_2$ (a); power angle of generator $G_1_G_3$ (b); bus 8 voltage (c); active power transmitted by tie line (d)

Table 4. System oscillation modes under the addition of energy storage

Model	λ	f (Hz)	ζ (%)	Attenuation coefficient	Mode
1	$-0.4970 \pm j4.092$	0.651	12.052	-0.497	1
	$-1.1124 \pm j7.197$	1.145	15.276	-1.112	2
	$-1.1024 \pm j7.208$	1.147	15.120	-1.102	3
2	$-0.5066 \pm j3.955$	0.629	12.705	-0.506	1
	$-1.0925 \pm j7.205$	1.147	14.991	-1.093	2
	$-1.1844 \pm j7.045$	1.121	16.579	-1.184	3
3	$-0.1085 \pm j3.722$	0.592	12.914	-0.108	1
	$-1.1399 \pm j7.184$	1.143	15.671	-1.140	2
	$-1.1855 \pm j7.062$	1.124	16.561	-1.186	3

oscillations of area 1, the damping ratios of the three models are similar. Model 3 has the best effect while model 2 has the lowest damping ratio, the highest frequency, the most rightward eigenvalues, the largest attenuation coefficient and the worst effect. For the oscillation mode of area 2, the damping effect of model 1 is the worst, while that of model 2 is the best, with the largest damping ratio and the smallest oscillation frequency. Therefore, the overall improvement effect of model 1 and model 2 is the most obvious.

4.2. Change the transmission power of the tie line

To reduce the power transmitted by the tie-line to 230 MW, the output of generators G_1 and G_2 are reduced to 620 MW and 600 MW, respectively. The corresponding active output power of generator G_4 at the slack node is 717 MW. A three-phase short-to-earth fault occurred at $t = 0.5$ s for the connection line between bus 7 and bus 8 was eliminated at $t = 0.51$ s. At $t = 2$ s, load 1 of bus 7 has a shock disturbance, and the active power and reactive power fluctuations are 5 MW and 10 MW, respectively. Then the load disturbance is eliminated at $t = 2.1$ s. At this time, the generator power angle and bus voltage are observed as shown in Fig. 9.

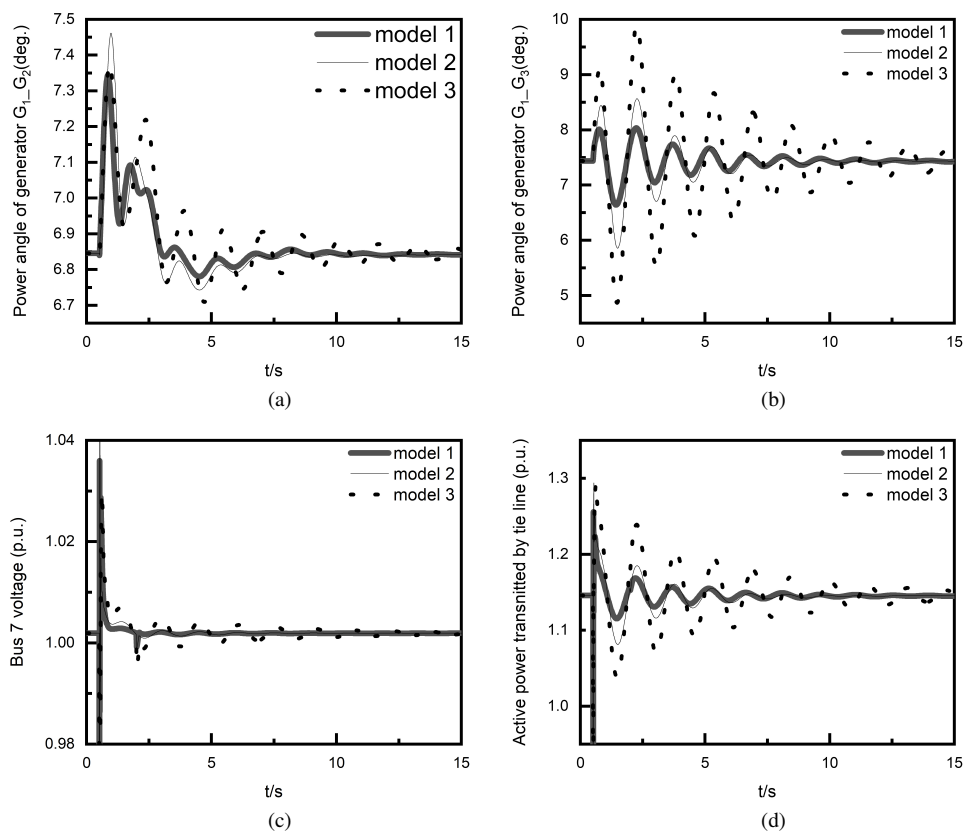


Fig. 9. Grid curve under energy storage after system transient fault: power angle of generator $G_1_{G_2}$ (a); power angle of generator $G_1_{G_3}$ (b); bus 7 voltage (c); active power transmitted by tie line (d)

It can be shown in Fig. 9 that under the condition of reducing the conventional generator output and transmission power, model 1 still has good stability in the event of system failure. The generator power angle fluctuation curve will recover steadily within 15 s, and the voltage of terminal bus 7 of the tie line recovers within 5 s. The power fluctuation and angle oscillation of the tie line in model 1 are the smallest, which can obviously suppress the output fluctuation and improve the system stability.

5. Simulation of Henan grid

5.1. Temporary single-phase short circuit grounding of the tie line

To test the performance of the model built in this paper in the large power grid, the Shihe-Chunshen line of a 500 kV double-circuit power grid in the Xinyang area of the Henan grid is taken as an example. As this line is located at the edge of the Henan grid, it is prone to stability problems. The main grid is shown in Fig. 10, where the Huayu power plant has four conventional generator units and the BESS is integrated with the Shihe power plant. The 500 kV line from Shihe to Chunshen transmits 325 MW of active power. To evaluate the effect of the control strategy on the system stability, the single-phase ground short circuit of the Shihe-Chunshen 500 kV line during the time from $t = 1$ s to $t = 1.01$ s as an example was taken, and the system simulation results are shown in Fig. 12.

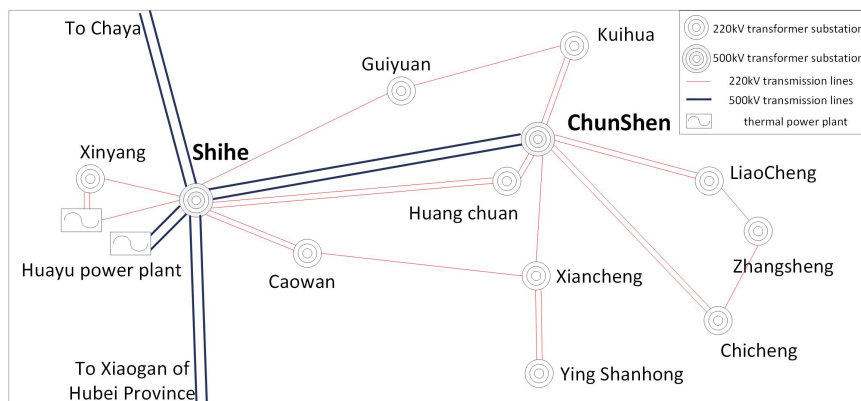


Fig. 10. Structure diagram of the grid of Xinyang District in Henan Power Grid

The simulation results of the integrated BESS shown in Fig. 10 illustrate that model 1 effectively contributes to the system damping and stabilizes system frequency within the primary frequency response.

The BESS integrated with the grid provides additional damping to support the system's stability. The associated bus voltage and generator frequency with the incorporated BESS are shown in Fig. 11 ((c) and (d)). It is observed that the BESS provides sufficient system damping and stabilizes the system response. The post-fault output responses of the system settle down

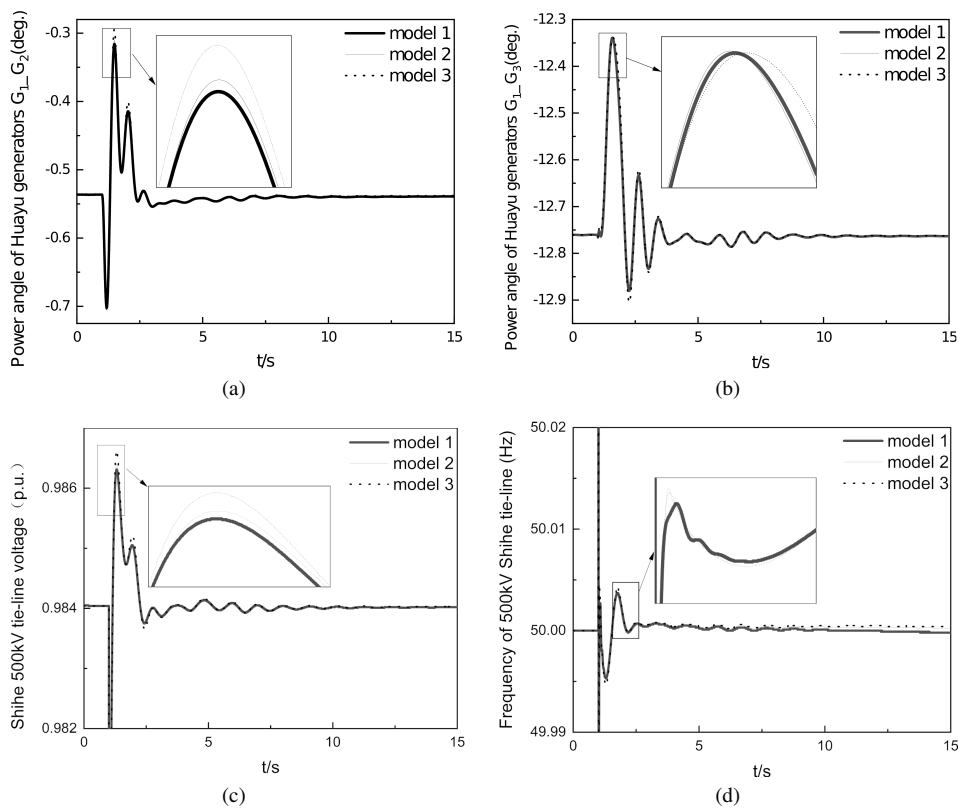


Fig. 11. Single-phase short-circuit ground fault simulation curve: power angle of Huayu generators $G_1_G_2$ (a); power angle of Huayu generator $G_1_G_3$ (b); Shihe 500 kV tie-line voltage (c); frequency of 500 kV Shihe tie-line (d)

within the specified stability recovery range. It also can be seen that the output deviation between three models is very small, but the BESS with VSG control is optimal.

5.2. Load step response at Chicheng station

In order to observe the system response under different stable operation points, the active power of Chicheng Station suddenly drops by 200 MW at $t = 1.2$ s and then remains unchanged. The active power output of energy storage is 1 MW, and the dynamic response of each energy storage model under the step response is shown in Fig. 12.

The system responses in Fig. 12 demonstrate that the difference between the three models is more pronounced when there is a step response to the grid load compared to a short circuit fault. The rotor angle of model 1 in Fig. 12(a) is significantly reduced and the time to suppress the system oscillation is reduced. The active power output of model 1 in Fig. 12(b) is stabilized at -23.6 MW after the oscillation, and the active power output of model 2 and model 3 decreases linearly. The bus frequency of model 2 and model 3 reaches a maximum value of 50.05 Hz

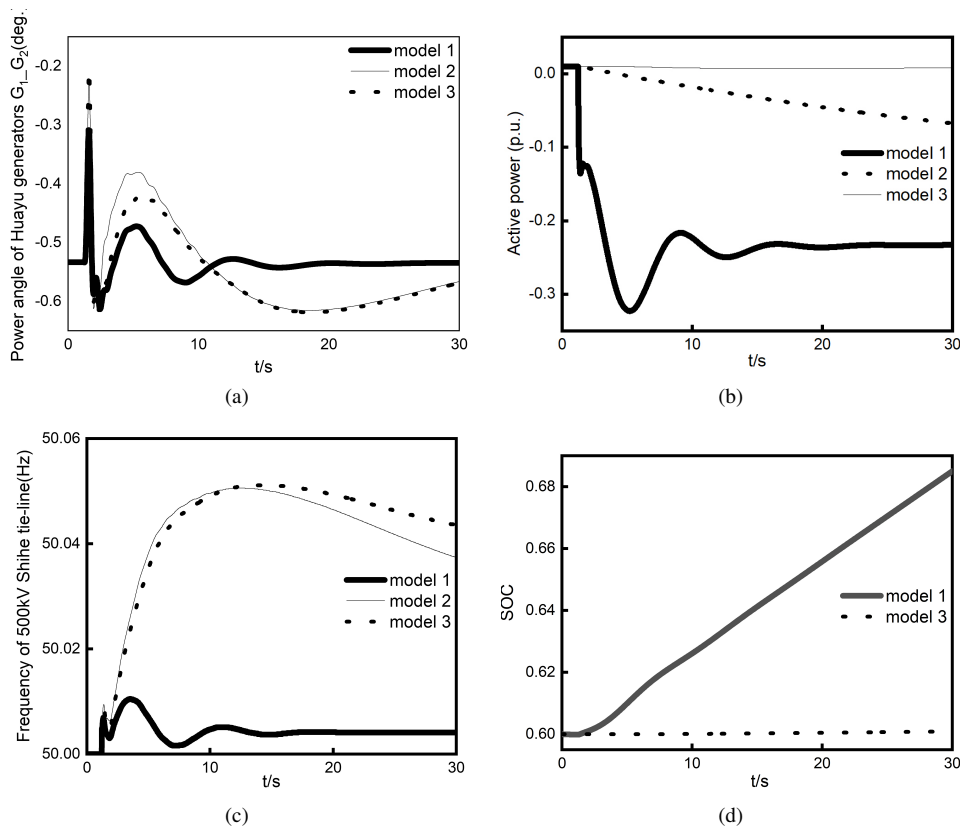


Fig. 12. Load step response simulation curve: power angle of Huayu generators $G_1_G_2$ (a); active power (b); frequency of 500 kV Shihe tie-line (c); SOC of BESS (d)

around $t = 12$ s, and then decreases slowly in Fig. 12(c). Model 1 reaches its maximum frequency deviation of 50.01 Hz at $t = 3.6$ s and then enters the steady-state at $t = 17$ s, reaching a new stable point. At this time, the system completes a frequency regulation and the bus frequency is 50.004 Hz. Due to the larger difference between the active power outputs of model 1 and model 3, the difference between the two in terms of SOC in (d) is also more significant.

The system responses demonstrate that the BESS with the proposed VSG control achieves power system stability. The effectiveness of VSG control in this case study is the same as in the case of the IEEE 4-machine 2-area system.

6. Conclusion

An energy storage electromechanical transient model is presented in this paper by introducing VSG control strategy which contains active frequency control, reactive voltage regulating control, virtual inertia control and a virtual damping model. The ontology model reflects the energy

storage efficiency, charging and discharging power limitation, charged limit condition and current transformer delay as well as the dead band. Based on the PSASP platform, the validity analysis is carried out on the IEEE 4-machine 2-area system and Henan grid to show its satisfying performance. The results show that the VSG strategy can improve the output fluctuation of the renewable energy unit, and the damping ratio of the inter-area oscillation mode of the system is significantly improved. The oscillation amplitude of the curve decreases and the stability time of the system is shortened.

Acknowledgements

The authors gratefully acknowledge the research funding provided by the National Natural Science Foundation of China (NSFC) (No. 51507157), the Scientific and Technological Research Foundation of Henan Province (No. 202102210305), the Institute Level Industrial Development Research Project (No. Y2021A-01), and the Project for University Key Teachers of Henan Province (2017GGJS093).

References

- [1] He P., Qi P., Ji Y.Q., *Dynamic interactions stability analysis of hybrid renewable energy system with SSSC*, Archives of Electrical Engineering, vol. 70, no. 2, pp. 445–462 (2021), DOI: [10.24425/aec.2021.136995](https://doi.org/10.24425/aec.2021.136995).
- [2] Lawder M.T., Suthar B., Northrop P.W.C., *Battery energy storage system (BESS) and battery management system (BMS) for grid-scale applications*, Proceedings of the IEEE, vol. 102, no. 6, pp. 1014–1030 (2014), DOI: [10.1109/JPROC.2014.2317451](https://doi.org/10.1109/JPROC.2014.2317451).
- [3] Zhao G.P., Shi L., Feng B., *Development Status and Comprehensive Evaluation Method of Battery Energy Storage Technology in Power System*, IEEE 3rd Information Technology, Networking, Electronic and Automation Control Conference (ITNEC), Chengdu, China, pp. 2080–2083 (2019), DOI: [10.1109/ITNEC.2019.8729448](https://doi.org/10.1109/ITNEC.2019.8729448).
- [4] Lee D.J., Wang L., *Small-signal stability analysis of an autonomous hybrid renewable energy power generation/energy storage system part i: time-domain simulations*, IEEE Transactions on Energy Conversion, vol. 23, no. 1, pp. 311–320 (2008), DOI: [10.1109/TEC.2007.914309](https://doi.org/10.1109/TEC.2007.914309).
- [5] Shim J.W., Verbic G., Kim H., *On droop control of energy-constrained battery energy storage systems for grid frequency regulation*, IEEE Access, vol. 7, pp. 166353–166364 (2019), DOI: [10.1109/ACCESS.2019.2953479](https://doi.org/10.1109/ACCESS.2019.2953479).
- [6] Zhang Y., Jiang Z.H., Yu X.W., *Control Strategies for Battery/Supercapacitor Hybrid Energy Storage Systems*, IEEE Energy 2030 Conference, GA, USA, pp. 1–6 (2008), DOI: [10.1109/ENERGY.2008.4781031](https://doi.org/10.1109/ENERGY.2008.4781031).
- [7] Hill C.A., Such M.C., Chen D., *Battery energy storage for enabling integration of distributed solar power generation*, IEEE Transactions on Smart Grid, vol. 3, no. 2, pp. 850–857 (2012), DOI: [10.1109/TSG.2012.2190113](https://doi.org/10.1109/TSG.2012.2190113).
- [8] Xu T., Jang W., Overbye T., *Commitment of fast-responding storage devices to mimic inertia for the enhancement of primary frequency response*, IEEE Transactions on Power Systems, vol. 33, no. 2, pp. 1219–1230 (2018), DOI: [10.1109/TPWRS.2017.2735990](https://doi.org/10.1109/TPWRS.2017.2735990).
- [9] Tamrakar U., Shrestha D., Maharjan M., *Virtual inertia: current trends and future directions*, Applied Sciences, vol. 7, no. 7, p. 654 (2017), DOI: [10.3390/app7070654](https://doi.org/10.3390/app7070654).
- [10] Kerdphol T., Rahman F.S., Watanabe M., *Enhanced virtual inertia control based on derivative technique to emulate simultaneous inertia and damping properties for microgrid frequency regulation*, IEEE Access, vol. 7, pp. 14422–14433 (2019), DOI: [10.1109/ACCESS.2019.2892747](https://doi.org/10.1109/ACCESS.2019.2892747).

- [11] Bevrani H., Ise T., Miura Y., *Virtual synchronous generators: A survey and new perspectives*. International Journal of Electrical Power and Energy Systems, vol. 54, no. 1, pp. 244–254 (2014), DOI: [10.1016/j.ijepes.2013.07.009](https://doi.org/10.1016/j.ijepes.2013.07.009).
- [12] Shi K., Ye H.H., Song W.T., *Virtual Inertia Control Strategy in Microgrid Based on Virtual Synchronous Generator Technology*, IEEE Access, vol. 6, pp. 27949–27957 (2018), DOI: [10.1109/ACCESS.2018.2839737](https://doi.org/10.1109/ACCESS.2018.2839737).
- [13] Wang Y., Liu B., Duan S., *Transient Performance Comparison of Modified VSG Controlled Grid-Tied Converter*, IEEE Applied Power Electronics Conference and Exposition (APEC), CA, USA, pp. 3300–3303 (2019), DOI: [10.1109/APEC.2019.8722121](https://doi.org/10.1109/APEC.2019.8722121).
- [14] Li H., Gu R.Z., *Research on Grid-connected Control and Simulation of Microgrid Inverter Based on VSG*, China International Conference on Electricity Distribution (CICED), Tianjin, China, pp. 2066–2070 (2018), DOI: [10.1109/CICED.2018.8592273](https://doi.org/10.1109/CICED.2018.8592273).
- [15] Liu X., Gong R., *A Control Strategy of Microgrid-Connected System Based on VSG*. In: International Conference on Power, Intelligent Computing and Systems (ICPICS), Shenyang, China, pp. 739–743 (2020), DOI: [10.1109/ICPICS50287.2020.9201955](https://doi.org/10.1109/ICPICS50287.2020.9201955).
- [16] Cheng C., Yang H., Zeng Z., *Rotor inertia adaptive control method of VSG*, Automation Electric Power Systems (in Chinese), vol. 39, no. 19, pp. 82–89 (2015), DOI: [10.7500/AEPS20141130003](https://doi.org/10.7500/AEPS20141130003).
- [17] *Power System Analysis Software Package User's Manual*, China, CEPRI, Beijing (2019).
- [18] How D., Hannan M.A., Lipu M.S.H., *State of charge estimation for lithium-ion batteries using model-based and data-driven methods: a review*, IEEE Access, vol. 7, pp. 136116–136136 (2019), DOI: [10.1109/ACCESS.2019.2942213](https://doi.org/10.1109/ACCESS.2019.2942213).
- [19] Ye X.H., Liu T., Wu G.Y., *Multi-time scale simulation modeling and characteristic analysis of large-scale grid-connected battery energy storage system*, Proceedings of the CSEE, vol. 35, no. 11, pp. 2635–2644 (2015), DOI: [10.13334/j.0258-8013.pcsee.2015.11.001](https://doi.org/10.13334/j.0258-8013.pcsee.2015.11.001) (in Chinese).
- [20] Liu M., Bizzarri F., Brambilla A., *On the impact of the dead-band of power system stabilizers and frequency regulation on power system stability*, IEEE Transactions on Power Systems, vol. 34, no. 5, pp. 3977–3979 (2019), DOI: [10.1109/TPWRS.2019.2920522](https://doi.org/10.1109/TPWRS.2019.2920522).